Diffusion-Limited Exciton-Exciton Annihilation in Carbon Nanotubes: Theoretical Model and its Comparison with Nonlinear Photoluminescence Experiment

Yoichi Murakami
Department of Chemical System Engineering, The University of Tokyo, 7-3-1 Hongo, Bunkyo-ku, Tokyo 113-8656, Japan
(Dated: June 10, 2019)

A theoretical model for describing the relationship between the intensity of photoluminescence (PL) emission from single-walled carbon nanotubes (SWNTs) and the intensity of the excitation light is developed for two limiting cases, the steady-state and instantaneous limits corresponding to CW and ultrashort-pulse excitations, respectively. The generation, relaxation, diffusion, and radiative and non-radiative decays of one-dimensional (1-D) excitons are taken into account. The developed model is compared and fitted to experimentally obtained "PL intensity vs. excitation intensity" curves, which allowed for the estimation of the exciton density in SWNTs. The model agrees with Monte Carlo calculations as well as with experimental results, from which the validity of the developed model was confirmed. It is shown that the solution obtained based on the conventional mean-field rate equation qualitatively disagrees with the experimental results in the high-saturation regime, which is considered to be due to the inherent collapse of the mean-field approximation for 1-D excitons.

PACS numbers: 78.67.Ch,71.35.-y,78.55.-m

I. INTRODUCTION

The optical and electronic properties of low-dimensional materials have been an important subject of study in the field of condensed matter physics. In particular, one-dimensional (1-D) materials are predicted to possess unique properties that are distinctly different from those at higher dimensions,[1,2] primarily due to the enhanced Coulomb interactions among the quantum confined charge carriers. One common feature of optically-excited low-dimensional systems is the formation of strongly bound electron-hole (e-h) pairs, or excitons,[3] which completely dominate interband optical spectra. 1-D semiconductors are expected to show an almost complete suppression of optical absorption at the band edges, with a significant fraction of oscillator strength taken by the lowest excitonic state.[4,5]

Early reports of lasing from semiconductor quantum wires (QWRs)[6,7] invoked much interest in the physics of *high density* 1-D excitons. A number of studies have thus far been performed on such QWRs during the last two decades to understand many-body phenomena (e.g., lasing, band-gap renormalization, biexciton formation, and the Mott transition),[8,9,10,11,12,13,14] but many aspects are still under debate. More recently, studies on high-density excitons have been extended to novel 1-D materials such as conjugated polymers[15,16,17,18] and single-walled carbon nanotubes (SWNTs).[19,20,21] Among them, SWNTs are an emerging 1-D material[22] attracting much interest from diverse research fields owing to their unique properties.[23] SWNTs are known to have extremely strong quantum confinement of ∼1 nm, giving rise to large exciton binding energies on the order of 0.5–1 eV,[24,25,26,27] much larger than those of GaAs QWRs (∼20 meV)[5,7] and comparable to or larger than those of conjugated polymers (∼0.4 eV[18] and <0.1 eV[28]).

Previously, we have investigated the properties of photoluminescence (PL) emission from high-density excitons in SWNTs through nonlinear photoluminescence excitation (PLE) spectroscopy using temporally-short optical pulses.[29] From the clear saturation of the intensities of all the PL features with increasing excitation laser intensity as well as the complete *flattening* of the PLE spectra at very high laser intensities, we showed the existence of an upper limit in the density of excitons that can be accommodated in SWNTs.[29] Such an upper limit has been considered to be imposed by the diffusive motion of excitons[30,31,32] combined with rapid and efficient exciton-exciton annihilation in SWNTs.[21]

In this report, a theoretical model describing the saturation behavior of the PL intensities is developed and compared with experimental results. In particular, the model takes into account the diffusive motion (or diffusion length) of excitons and exciton-exciton annihilation (EEA) to describe diffusion-limited EEA in SWNTs. Regarding the diffusion-limited particle annihilation/reaction problems in 1-D, so far numerous theoretical studies have been reported[33,34,35,36,37,38,39] that describe analytical solutions for the temporal decay dynamics of the particle populations in respective systems. The model introduced in this report provides the direct analytical solution for the relationship between the intensity of the excitation light ($I_{\rm pump}$) and that of the emitted PL ($I_{\rm PL}$), which provides us a convenient way to quantitatively estimate the density of excitons by fitting the model solution to the experimentally obtained $I_{\rm pump}$ vs. $I_{\rm PL}$ curves.

In the first part (Section II), the details of the performed experiment and the relevant results are presented. Subsequently (Section III), the theoretical model is developed and introduced in detail. The model is compared with experimental results, a Monte Carlo simulation, and

the solution of the conventional EEA rate equation in Section IV, along with discussions. Finally, a summary is given in Section V.

II. EXPERIMENT

A. Detail of experimental methods

The sample studied was prepared by ultrasonicating CoMoCAT SWNTs in D_2O with 1 wt% sodium cholate surfactant by a horn-type ultrasonicator for 30 min and subsequently ultracentrifuged at 111,000 g for 4 h. The upper 50% supernatant was taken out from the centrifuge tubes. The solution was put in a 1-mm-thick quartz cuvette. The optical density of the sample around the E_{22} resonance (500–700 nm range) was less than 0.2, which helped avoid non-uniform excitation and re-absorption of the emitted PL within the sample. The excitation source was an optical parametric amplifier (OPA), producing ∼250 fs pulses at a repetition rate of 1 kHz tunable in the visible and near-infrared ranges, pumped by a chirped-pulse amplifier (Clark-MXR, Inc., CPA-2010). Optical filters were carefully selected and set in the beam path to thoroughly eliminate any parasitic wavelength components contained in the OPA beam (primarily in the ultraviolet and near-infrared regions). The beam was focused onto the sample to a spot size of 300–400 μm. Only the central portion of the OPA beam profile (diameter: $\approx$ 6 mm) was selected by placing a round aperture (diameter: $\approx$ 2 mm) just before the focus to enhance the spot uniformity at the sample. The PL from the sample was focused onto the monochromator entrance and recorded with a liquid-nitrogen-cooled InGaAs array detector. The obtained PL spectra were corrected for the wavelength-dependence of the grating efficiency and detector sensitivity.

For the data shown in Fig. 1(c), a different sample as well as a different excitation light source was used to verify the universality of the phenomena observed. In this case, the sample was a dried film of CoMoCAT SWNTs embedded in ι-carrageenan, formed by drying a mixed gel of ι-carrageenan and centrifuged supernatant of CoMoCAT SWNTs on the surface of a sapphire substrate. The sapphire substrate served as a mechanical support as well as a heat sink for the film during the measurements. The excitation light was ∼250 fs optical pulses (1 kHz pulse frequency) with a central wavelength of 653 nm (FWHM = 10 nm), produced by filtering whitelight pulses generated by focusing the CPA beam onto a sapphire crystal.

B. Experimental results

Figure 1(a) compares two PL spectra. The black solid curve was obtained using the OPA with a wavelength of 654 nm (1.90 eV) and a pulse energy of 29 nJ, while the red dotted curve was obtained using a weak (100 μW)

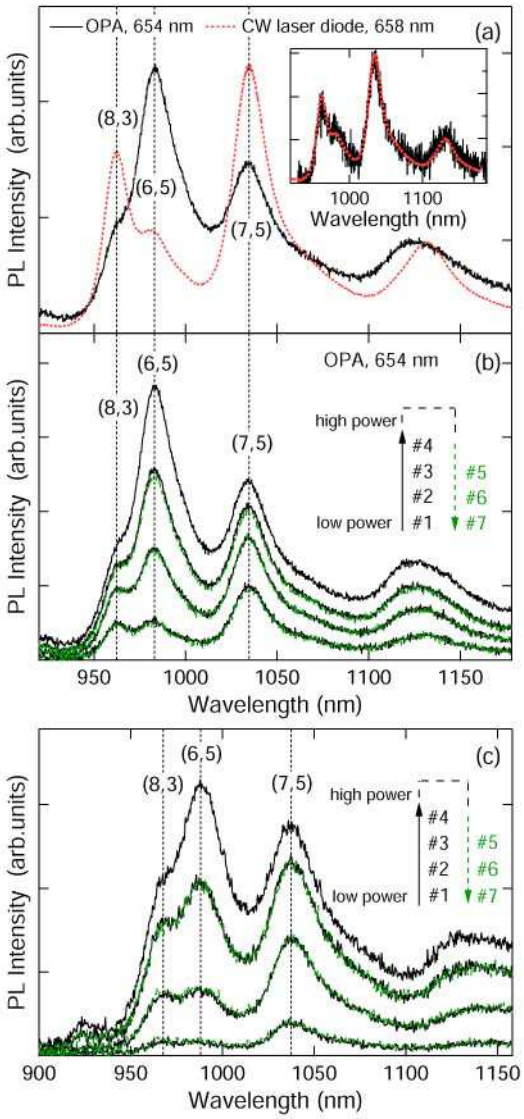

FIG. 1: (color online) Pump-intensity-dependent PL spectra measured for (a, b) the centrifuged supernatant of CoMoCAT SWNTs dispersed in D_2O and (c) CoMoCAT SWNTs embedded in a dried ι-carrageenan film. (a) Black solid curve is spectrum obtained with OPA pulse (654 nm, 29 nJ). Red dotted curve is spectrum obtained with a CW laser diode (658 nm, 100 μW). Inset shows that the two spectra coincide when the OPA pulse energy is very low (300 pJ). (b) Change of PL spectra with pulse energy of the OPA beam (654 nm) varied between 1 and 30 nJ in the order of #1 to #7. Curve #4 corresponds to the highest fluence ($\sim 1.3 \times 10^{14}$ photons/cm^2). (c) Change of PL spectra with the pulse energy of 653 nm light (FWHM = 10 nm) varied between 1 and 20 nJ in the order of #1 to #7. In panels (b) and (c), the relative magnitudes along the ordinate axis are preserved among the spectra, and thus represents actual intensity ratios.

CW laser with a wavelength of 658 nm (1.88 eV). It is seen that the relative intensities of different PL peaks are drastically different between the two curves. The inset confirms that the two spectra actually coincide very accurately when the OPA pulse energy is kept very low (300 pJ). Figure 1(b) shows PL spectra measured with pulse energies of 1 nJ (curves #1 and #7), 4 nJ (#2 and #6), 10 nJ (#3 and #5), and 30 nJ (#4). The (7,5) peak is dominant at low fluences while the (6,5) peak becomes dominant at high fluences. It is important to note that the measurements were taken in the order of #1 to #7, demonstrating that the observed changes are reproducible and are not caused by any laser-induced permanent change in the sample. Additionally, note that the PL intensities tend to saturate at high laser fluences, while their peak positions remain unchanged.

Figure 1(c) shows PL spectra measured for the dried ι-carrageenan film using 653 nm optical pulses with a FWHM bandwidth of 10 nm at different pulse energies. The pulse energies were 1 nJ (curves #1 and #7), 3 nJ (#2 and #6), 10 nJ (#3 and #5), and 20 nJ (#4) measured in the order of #1 to #7. Figure 1(c) exhibits the same behavior as that shown in Fig. 1(b), demonstrating that the observed changes shown in Fig. 1(b) did not result from any artifacts, e.g., caused by the fluidic nature of the sample or by the unnoticed parasitic wavelength components in the OPA beam.

In order to obtain PL intensity (I_{PL}) versus pump intensity (I_{pump}) relationships for different emission peaks, PL spectra at different photon fluences were measured for various excitation wavelengths. Photon fluence [number of photons/cm^2] is used to denote the intensity of excitation pulses, hereafter. Each PL spectrum was decomposed and fitted by multiple peaks corresponding to the SWNT types/chiralities involved in the measured wavelength range. A 50% Gaussian + 50% Lorentzian lineshape was assumed, and the decomposition was performed by optimizing the peak-width so that the decomposition yielded the best fitting for the original PL spectrum. The optimum widths at the highest fluence were ~15% larger than those at the lowest fluence in Fig. 1, and such an increment of the width is considered to be caused by the enhanced interactions among excitons or their reduced lifetime due to the high exciton density. Throughout the decomposition analysis, peak positions of all the PL features and the ratios among their widths were fixed regardless of the excitation wavelength and photon fluence.

Figure 2 shows the obtained integrated PL peak intensities (I_{PL}) plotted against the incident photon fluence (I_{pump}) for (6,5), (7,5), and (8,3) SWNTs at excitation wavelengths of 570, 615, and 658 nm. The resonance wavelengths of these SWNT types at the E_{22} levels are approximately 570, 647, and 673 nm, respectively. It can be seen that the integrated PL intensity begins to saturate at a lower (higher) fluence when SWNTs are excited resonantly (non-resonantly). Unexpectedly fast saturation of the PL from (7,5) with 570 nm excitation (which

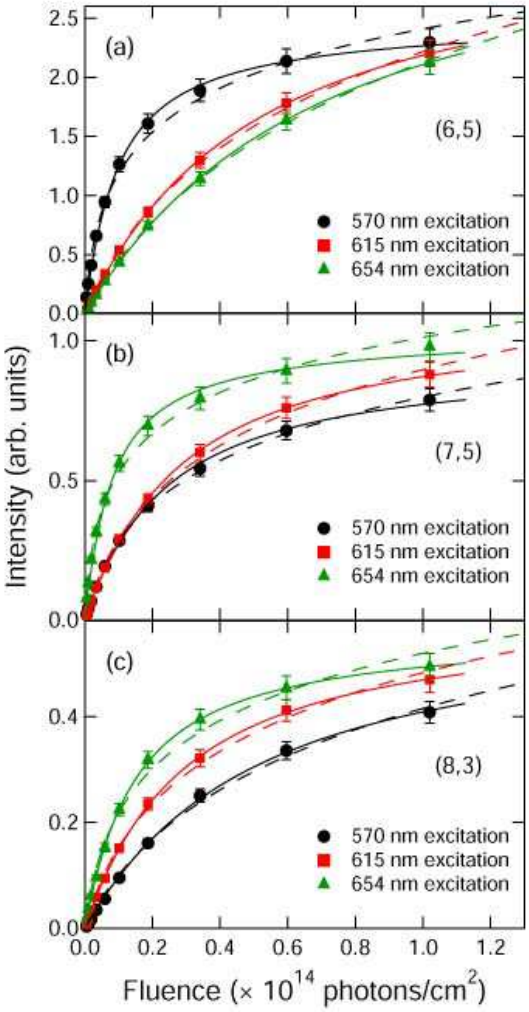

FIG. 2: (color online) Integrated PL intensity versus pump fluence for (6,5), (7,5), and (8,3) SWNTs. Pump wavelengths were 570 nm (circles), 615 nm (squares), and 654 nm (triangles). The error bars account for ±5%. The solid and dashed curves are fittings by Eq. (15) and Eq. (19), respectively.

is non-resonant) can be attributed to its proximity to the phonon sideband at ~585 nm.[40]

Based on further experimental support,[29] we interpret these observations as results of very efficient exciton-exciton annihilation (EEA),[15,16,17,18,21,33] a non-radiative process that occurs at high exciton densities where two excitons are spatially close enough to interact with each other, resulting in the annihilation of the two excitons and simultaneous creation of an *e-h* pair in a higher energy state (either as a bound exciton or a free *e-h* pair). Briefly, we observed flattening of the PLE spectra *and* the invariance of the optical transmission spectrum (both were measured using the same optical pulses for E_{22} range), which clearly demonstrate that *this PL saturation was not caused by phase-space filling.* More importantly, this demonstrates the existence of an upper limit in the density of excitons in SWNTs, where

such an upper limit is considered to be caused by EAA that serves as a bottleneck for the exciton density.[29]

III. MODEL

In this section, a theoretical model for explaining the experimental results is described, taking into account the generation, relaxation, diffusion, and radiative and non-radiative decays of 1-D excitons. As shown below, this model allows us to simulate saturation curves for $I_{\rm PL}$ as a function of $I_{\rm pump}$ in two limiting cases. It also provides an estimate for the exciton density in the saturation regime for a given average diffusion length of excitons within the spontaneous decay lifetime (or, for a given diffusion constant of excitons, if the spontaneous decay lifetime is known).

A. Model basis and assumptions

Figure 3(a) shows a schematic energy diagram of the excitons in semiconducting SWNTs under consideration. We are interested in calculating the population of excitons N (indicated by the dotted box) in the lowest energy state E_{11}. First, excitons are created by optical excitation at an energy around the E_{22} level, which is typically in the visible wavelength range. The excitation intensity is denoted by $I_{\rm pump}$. As soon as excitons are created they decay to the E_{11} level within a very short time ($\sim$40 fs)[41] by transferring their energies to the lattice. Recent studies have reported that the excitons created around E_{22} levels primarily decay to the E_{11} level with a probability close to unity.[42,43] The influx of excitons to the E_{11} level is denoted $G_{\rm in}$. On the other hand, the spontaneous decay time $\tau_{\rm tot}$ of the E_{11} excitons to the ground state (G.S.) has been reported to be 10–100 ps.[44,45,46] Such a spontaneous decay consists of radiative and non-radiative processes, with respective rates $\gamma_{\rm r}$ and $\gamma_{\rm nr}$ [s^{-1}], where $\gamma_{\rm r}+\gamma_{\rm nr} \equiv \gamma_{\rm tot} = {\tau_{\rm tot}}^{-1}$. The outflux of excitons from the E_{11} level *via the spontaneous decay process* is denoted by $G_{\rm out}$. Therefore, the flux of the PL photons or the PL intensity ($I_{\rm PL}$) is equal to $\eta G_{\rm out}$, where η ($\equiv \gamma_{\rm r}/\gamma_{\rm tot}$) denotes the branching ratio for the radiative decay from the E_{11} level.

As the density of excitons increases, the EEA process becomes important. If the *e-h* pair created in the higher energy state returns back to the E_{11} exciton level with a probability of λ ($0 \le \lambda \le 1$), the initial two excitons are eventually reduced to λ excitons (as an expectation value) through such an EEA process. The following two assumptions are made: (1) Once two excitons intersect in a SWNT, EEA occurs instantaneously with a probability of one; (2) the spatial positions where excitons are created in SWNTs by optical excitations are random.

Figure 3(b) schematically shows a situation in which N excitons exist in a SWNT of length of L. Each exciton is considered to "occupy" a characteristic length $l_{\rm x}$

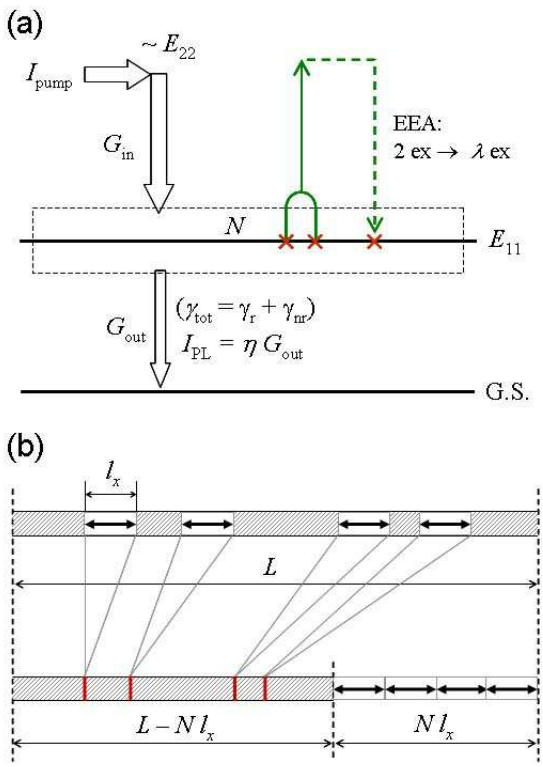

FIG. 3: (color online) (a) Schematic energy diagram of the system considered in the model. The dotted box enclosing the lowest energy level (E_{11}) is the domain of interest where N excitons are populated. All the symbols are defined in the text. (b) Schematic description of $N = 4$ excitons randomly distributed over a SWNT with a length of L. The horizontal arrow with a length of $l_{\rm x}$ denotes the average length traversed by one exciton during its spontaneous decay lifetime $\tau_{\rm tot}$. The lower part is the equivalent of the upper but emphasizes that the total length of the unoccupied region is $L - N l_{\rm x}$ where N vertical thick bars denote the borders of the areas occupied by those excitons. The ends of the SWNT are assumed to be a cyclic boundary.

in a SWNT. Specifically, $l_{\rm x}$ is assumed to be the average length traveled by an exciton during the spontaneous decay lifetime $\tau_{\rm tot}$ and is written as $\sqrt{D\tau_{\rm tot}}$, where D [cm^{-1}] is the exciton diffusion constant. Namely, it is assumed that $l_{\rm x}$ is determined by the diffusion length, and any two excitons created within $l_{\rm x}$ undergo EEA.

First, a 1-D space of length L is considered where N segments (or excitons) of length $l_{\rm x}$ are randomly present without overlapping each other, as shown in Fig. 3(b). The probability of a new segment (of length $l_{\rm x}$) to enter the system *without* overlapping any of the N existing segments, $p(N)$, is given by the product of the following two probabilities

$$p_1 = 1 - \frac{N l_{\rm x}}{L} \qquad (1)$$

which is the probability for the center of the new segment to land on an unoccupied area [hatched regions in

Fig. 3(b)], and

$$p_2 = \left(1 - \frac{l_x}{L - N l_x}\right)^N \tag{2}$$

which is the probability that the occupying length (l_x) of the new segment (whose center has landed on an unoccupied area) does not interfere with any of the N existing segments [vertical thick bars in the lower part of Fig. 3(b)]. Hence, $p(N)$ is written as

$$p(N) = \left(1 - \frac{N l_x}{L}\right)\left(1 - \frac{l_x}{L - N l_x}\right)^N . \tag{3}$$

The expectation value of the increment of N due to the introduction of a new segment into the system, $\langle \Delta N \rangle_N$ ($0 < \langle \Delta N \rangle_N \leq 1$), depends on the type of two-particle annihilation considered. For the general "$ex + ex \rightarrow \lambda ex$" case, $\langle \Delta N \rangle_N$ is expressed as

$$\langle \Delta N \rangle_N = p(N) - (1 - \lambda)(1 - p(N)) . \tag{4}$$

In the following, the derivation for the case of $\lambda = 1$ is shown as a specific example. The final results will be presented for both the $\lambda = 1$ and $\lambda = 0$ cases.

B. Solutions in limiting cases

1. Steady-state limit

The *steady-state* limit is considered here, in which the number of excitons N in the system is steady, corresponding to CW excitation. In order to derive the relationship between $I_{\rm pump}$ and $I_{\rm PL}$, let us consider the relationship between $G_{\rm in}$ and $G_{\rm out}$ [see Fig. 3(a)], where both $G_{\rm in}$ and $G_{\rm out}$ are *rates*, having units of [s^{-1}]. When N is sufficiently small and EEA is negligible, $G_{\rm in} = G_{\rm out} = \gamma_{\rm tot} N$. When EEA is present, however, this relationship becomes

$$G_{\rm in} = \frac{G_{\rm out}}{\langle \Delta N \rangle_N} = \frac{\gamma_{\rm tot} N}{\langle \Delta N \rangle_N} . \tag{5}$$

In the case of $\lambda = 1$, Eq. (4) and Eq. (5) lead to

$$G_{\rm in} = \frac{\gamma_{\rm tot} N}{\left(1 - \frac{N l_x}{L}\right)\left\{1 - \frac{l_x}{L}\left(1 - \frac{N l_x}{L}\right)^{-1}\right\}^N} . \tag{6}$$

Two dimensionless variables $\zeta \equiv N l_x / L$ and $\psi \equiv G_{\rm in} l_x / \gamma_{\rm tot} L$ are introduced, the former of which is a dimensionless exciton population ($0 \leq \zeta < 1$). Using these variables, Eq. (6) can then be rewritten in dimensionless form:

$$\psi = \frac{\zeta}{(1 - \zeta)\left\{1 - \frac{l_x}{L}(1 - \zeta)^{-1}\right\}^{\frac{L}{l_x}\zeta}} . \tag{7}$$

Expanding the second factor in the denominator of Eq. (7) and eliminating higher-order terms of l_x/L leads to an equation of only ζ and ψ, expressed as

$$\psi = \frac{\zeta}{(1 - \zeta)\sum_{\kappa=0}^{\infty} \frac{(-1)^\kappa}{\kappa!}\left(\frac{\zeta}{1-\zeta}\right)^\kappa} . \tag{8}$$

Summing up to $\kappa = 5$ in Eq. (8) is usually sufficient to reproduce Eq. (7) for $l_x/L \leq 0.1$. Finally, noting that the denominator of Eq. (8) is equal to the Taylor expansion of an exponential function, the solution for the steady-state limit for $\lambda = 1$ ($ex + ex \rightarrow ex$) is expressed as

$$\psi = \frac{\zeta}{1 - \zeta} \exp\left(\frac{\zeta}{1 - \zeta}\right) . \tag{9}$$

Here, since $I_{\rm PL} \propto N$ and $I_{\rm pump} \propto G_{\rm in}$, $I_{\rm PL}$ and $I_{\rm pump}$ are proportional to ζ and ψ, respectively, i.e., $I_{\rm PL} = c_1 \zeta$ and $I_{\rm pump} = c_2 \psi$, where c_1 and c_2 are real constants.

On the other hand, the solution for the case of $\lambda = 0$ ($ex + ex \rightarrow 0$) is derived through a similar procedure, yielding

$$\psi = \frac{\zeta}{2(1 - \zeta)\exp\left(-\frac{\zeta}{1-\zeta}\right) - 1} . \tag{10}$$

Equations (9) and (10), valid for CW PL experiments, are implicit equations relating the PL intensity ($I_{\rm PL}$) and the pump intensity ($I_{\rm pump}$) in terms of their respective dimensionless variables ζ and ψ. These equations contain no fitting parameters except the two linear scaling factors c_1 and c_2 and simply become equivalent ($\zeta = \psi$) in the low density limit ($\zeta \rightarrow 0$).

2. Instantaneous limit

Here, the *instantaneous* limit is considered in which all the excitons are created at $t = 0$ with an infinitesimally short optical pulse, and then the intraband relaxation and EEA follow immediately. This limit represents a situation where the duration of the optical pulse and the time required for intraband relaxation and EEA process are much shorter than the spontaneous decay time $\tau_{\rm tot}$, as in the case of the present experimental situation. The pump intensity $I_{\rm pump}$ in this limit is directly proportional to N_0, the number of excitons or e-h pairs created at $t = 0$, while the PL intensity $I_{\rm PL}$ is proportional to the number of excitons N that survived EEA. The relationship between N_0 and N is described by the differential equation

$$dN_0 = \frac{dN}{\langle \Delta N \rangle_N} \tag{11}$$

where $\langle \Delta N \rangle_N$ is given by Eq. (4). When $\lambda = 1$ is assumed, Eq. (11) is rewritten as

$$\frac{dN_0}{dN} = \frac{1}{\left(1 - \frac{N l_x}{L}\right)\left\{1 - \frac{l_x}{L}\left(1 - \frac{N l_x}{L}\right)^{-1}\right\}^N} . \tag{12}$$

As in the previous case (steady-state limit), dimensionless variables $\zeta \equiv N l_{\rm x}/L$ and $\psi \equiv N_0 l_{\rm x}/L$ are introduced. Again, since $I_{\rm PL} \propto N$ and $I_{\rm pump} \propto N_0$, $I_{\rm PL} = c_1\zeta$ and $I_{\rm pump} = c_2\psi$, where c_1 and c_2 are constants. With ζ and ψ, Eq. (12) can be written in a dimensionless form:

$$\frac{d\psi}{d\zeta} = \frac{1}{(1-\zeta)\left\{1-\frac{l_{\rm x}}{L}(1-\zeta)^{-1}\right\}^{\frac{L}{l_{\rm x}}\zeta}}. \qquad (13)$$

Furthermore, similar to the steady-state case, an expansion is performed on the denominator of Eq. (13) together with elimination of the higher-order terms of $l_{\rm x}/L$, resulting in a differential equation of only ζ and ψ:

$$\frac{d\psi}{d\zeta} = \frac{1}{1-\zeta}\exp\left(\frac{\zeta}{1-\zeta}\right). \qquad (14)$$

Finally, by integrating Eq. (14) from 0 to ζ, the solution for $\lambda = 1$ ($ex + ex \rightarrow ex$) is obtained

$$\psi = \frac{1}{e}\left\{\mathrm{Ei}\left(\frac{1}{1-\zeta}\right) - \mathrm{Ei}(1)\right\}. \qquad (15)$$

Similarly, the solution for $\lambda = 0$ ($ex + ex \rightarrow 0$) in the instantaneous limit is

$$\psi = \int_0^\zeta \frac{1}{2(1-\zeta)\exp\left(-\frac{1}{1-\zeta}\right) - 1} d\zeta \qquad (16)$$

where the integral has to be solved numerically. Equations (15) and (16) become equivalent ($\zeta = \psi$) in the low density limit ($\zeta \rightarrow 0$).

IV. COMPARISONS AND DISCUSSIONS

A. Comparison of Model and Experiment

To compare with the experimental data shown in Fig. 2, Eq. (15), which is for the instantaneous limit with $\lambda = 1$, is used. The choice of this equation is because of the short duration of the optical pulses used (∼250 fs), the very fast (∼40 fs[41]) and efficient[42,43] internal decay of excitons created at E_{22} levels to the lowest E_{11} level, and the much longer spontaneous decay time from the E_{11} level (10–100 ps).[44,45,46] The solid curves shown in Fig. 2 were fit using Eq. (15), indicating that the model agrees well with the experimentally observed PL saturation behavior.

Table I is a summary of the fitting analysis performed on the data in Fig. 2 using Eq. (15). The first two columns show the optimum values of the scaling factors c_1 and ${c_2}^{-1}$. These are thought to be proportional to the oscillator strength for the PL emission from E_{11} levels and the oscillator strength for the optical absorption around E_{22} levels, respectively, as expected from $I_{\rm PL} \propto c_1 N$ and $N_0 \propto {c_2}^{-1} I_{\rm pump}$. The right three columns (ζ, N, and R) are values at 1.02×10^{14} photons/cm^2 (see Fig. 2). The values of N were obtained through the relationship $N = \zeta/l_{\rm x}$, where $l_{\rm x}$ was assumed to be 45 nm (one half of the average exciton excursion range defined in Ref. 32). The exciton density in the highly saturated regime ($\sim 1 \times 10^5$ cm^{-1}) is still more than one order magnitude smaller than the expected Mott density in SWNTs ($\sim 7 \times 10^6$ cm^{-1}, assuming an exciton size of ∼1.5 nm)[25], as has been discussed in detail in Ref. 29. R in the right-most column denotes the ratio between the number of as-created e-h pairs and the number of excitons that survived the EEA process until their spontaneous decay to the ground state, or N_0/N. The values of R show that approximately 90% of the initially created e-h pairs/excitons decay non-radiatively through the EEA path when the E_{22} levels are resonantly excited at a fluence of 1.02×10^{14} photons/cm^2.

Type	Exct. (nm)	c_1 ($\times 10^5$)	${c_2}^{-1}$ ($\times 10^{-14}$)	ζ	N ($\times 10^5$ cm^{-1})	R
(6,5)	570	2.97	7.74	0.764	1.70	10.3
	615	3.89	1.54	0.566	1.26	2.78
	654	4.21	1.13	0.505	1.12	2.28
(7,5)	570	1.14	3.18	0.678	1.51	4.77
	615	1.34	2.68	0.656	1.46	4.17
	654	1.22	9.16	0.776	1.72	12.0
(8,3)	570	0.73	1.54	0.566	1.26	2.78
	615	0.72	2.61	0.652	1.45	4.07
	654	0.68	5.05	0.729	1.62	7.05

TABLE I: Summary of the optimal parameters to used fit the experimental data, obtained from the analysis with Eq. (15). ζ, N, and R are values at the fluence of 1.02×10^{14} photons/cm^2, corresponding to the largest fluence in Fig. 2.

As expected, the values of c_1 are similar within the same chirality type, regardless of the excitation wavelength. However, for the particular case of (6,5) with 570 nm excitation, where the excitation wavelength exactly coincided with the E_{22} resonance peak, the value of c_1 ($\sim 3 \times 10^5$) is appreciably smaller than those at the other excitation wavelengths ($\sim 4 \times 10^5$). Such a small c_1 value implies that more excitons decayed to the G.S. through non-radiative paths compared to the other cases. This may be due to an emergence of stronger nonlinear processes that have not been taken into account in the assumptions, such as the breakdown of the $\lambda = 1$ assumption and/or the appearance of *more-than-two*-body annihilation processes because of the very high initial e-h pair density, achieved with the strong E_{22} resonance in this particular case.

The values of ${c_2}^{-1}$ also show the expected tendency toward higher (lower) values when the excitation wavelength is closer to (further from) the E_{22} resonance wavelength. The slightly higher ${c_2}^{-1}$ value for the case of (7,5) with 570 nm excitation is again attributed to its vicinity to the E_{22} phonon sideband at ∼585 nm.[40]

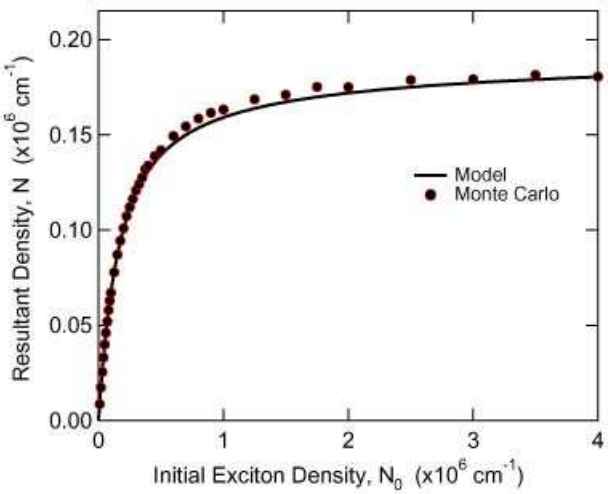

FIG. 4: (color online). Comparison between the saturation behavior predicted by Eq. (15) (black solid curve) and the result obtained by a Monte Carlo simulation of the EEA process. The abscissa denotes the density of initially created excitons while the ordinate corresponds to the resultant density. The experimental range of N_0 in Fig. 2 is $N_0 \leq 2 \times 10^6$ cm^{-1}.

B. Comparison with Monte Carlo Calculation

To further confirm the validity of the model, a computational simulation was performed based on the Monte Carlo method. At the beginning of the simulation, a random distribution of N_0 excitons along a line is created at time $t = 0$, corresponding to the instantaneous limit. For $t > 0$, each exciton undergoes a random movement in each computational step dt by the distance given by the probability distribution of $\bar{N}(0, l_0^2)$, where $\bar{N}(x_0, \sigma^2)$ denotes the normal distribution centered at x_0 with variance σ and $l_0 \equiv \sqrt{Ddt}$. Upon intersection of any two excitons, the EEA of $\{ex + ex \rightarrow ex\}$ takes place. In addition, each exciton is eliminated from the system with a probability of $\gamma_{\rm tot}dt$ $(= {\tau_{\rm tot}}^{-1}dt)$, corresponding to possible spontaneous decay during each computational step.

Figure 4 shows a comparison between the model for the instantaneous limit [Eq. (15)] with $l_{\rm x} = 45$ nm and the result of the Monte Carlo simulation, plotting the relationship of N_0 and N. The simulation was performed with $D = 0.42$ cm^2/s and $\tau_{\rm tot} = 100$ ps, which resulted in an average exciton displacement of 45 nm based on the same simulation performed without EEA.[47] The comparison shows satisfactory agreement, indicating that the simple analytical form of Eq. (15) well describes the phenomenon of diffusion-limited EEA, hence validating the proposed model.

C. Comparison with Conventional Rate-Equation Solution

Conventionally, a rate equation of the form

$$\frac{dN(t)}{dt} = G_{\rm in}(t) - \gamma_{\rm tot}N(t) - \gamma_{\rm EEA}N(t)^2 \qquad (17)$$

has been used to explain EEA processes observed for various materials from 1-D to 3-D.[16,17,18,21,48,49,50] The terms on the right hand side, from left to right, represent the rate of excitons entering the system (or the E_{11} level in the present case), the rate of excitons spontaneously decaying from the system to the ground state at a rate of $\gamma_{\rm tot}$, and the rate of excitons leaving the system because of EEA at a rate of $\gamma_{\rm EEA}$, respectively. This equation is the so-called "mean-field rate equation"[36,37], in which the spatial distribution of particles is described in terms of the *mean density* $N(x,t)$ or its further spatially-averaged form of $N(t)$ as in Eq. (17). Under this assumption, the possibility of finding two excitons at the same position or EEA rate has been assumed to be proportional to N^2, and hence the actual discrete distribution as well as the finite occupying sizes of the particles in 1-D space has been neglected. Although conventionally used, the decay dynamics of the particle population by two-body annihilations predicted based on the mean-field assumption is known to be incorrect for dimensions less than two.[33,35,36,37]

Equation (17) is solved for the pulse-wise creation of N_0 excitons at $t = 0$ [i.e., $G_{\rm in}(t) = \delta(N_0)$] in order to be compared with the proposed model for the instantaneous limit [Eq. (15)] and the experimental results. With this initial condition, Eq. (17) is readily solved to be

$$N(t) = \frac{1}{\left(\frac{1}{N_0} + \Gamma\right)\exp\left(\gamma_{\rm tot}t\right) - \Gamma} \quad \left[\Gamma \equiv \frac{\gamma_{\rm EEA}}{\gamma_{\rm tot}}\right] . \quad (18)$$

The total number of photons emitted from the sample $I_{\rm PL}$ is obtained by integrating Eq. (18) from $t = 0$ to ∞ as

$$I_{\rm PL} = \eta\int_0^\infty \gamma_{\rm tot}N(t)dt = -\frac{\eta}{\Gamma}\ln\left\{1 - \left(1 + \frac{1}{N_0\Gamma}\right)^{-1}\right\} \qquad (19)$$

where $\eta = \gamma_{\rm r}/\gamma_{\rm tot}$ as before. Equation (19) describes the relationship between $I_{\rm PL}$ and N_0 in terms of two adjustable components η/Γ and $N_0\Gamma$.

The dashed lines drawn in Fig. 2 are the optimum fits by Eq. (19) to the experimental data. While Eq. (19) reproduces the behavior well for the regime of weaker PL saturation with non-resonant excitations, the deviation becomes clearer for the regime of stronger PL saturation with resonant excitations. The most important *qualitative* difference between the two cases is that, while an upper limit in the density of excitons should exist in 1-D, as has clearly been supported by experiment[29] and the Monte Carlo simulation shown in Fig. 4, the density

predicted by Eq. (19) has *no upper limit* as recognized by the steadily increasing dashed lines shown in Fig. 2 and the logarithmic form of Eq. (19). Although the mean-field assumption in Eq. (17) may work as an approximation when the initial particle density N_0 (more precisely, the dimensionless initial density $N_0\sqrt{D\tau_{\rm tot}}$) is sufficiently low,[33] its validity collapses when the initial density is not low and hence the fluctuation in the resultant particle distribution becomes prominent with progressing t.[36]

Another important difference between Eq. (15) and Eq. (19) is described as follows: The solution of the conventional rate equation [Eq. (19)] contains two independent quantities: η/Γ and $N_0\Gamma$. The former can be used to scale $I_{\rm PL}$. However, since the parameter $N_0\Gamma$ simultaneously scales $I_{\rm pump}$ ($\propto N_0$) *and* changes the shape of the saturation curve, one essentially cannot estimate the density of excitons from the fitting analysis based on Eq. (19). On the other hand, since the shape of Eq. (15) has been uniquely determined, the only thing one can do is to *linearly and independently* change the two scaling constants c_1 and c_2 for $I_{\rm PL}$ and $I_{\rm pump}$, respectively, yielding sets of ζ and ψ values along the scaled (or fitted) $I_{\rm PL}$ vs. $I_{\rm pump}$ curves.

V. SUMMARY

A theoretical model has been developed for describing the relationship between PL intensity ($I_{\rm PL}$) and intensity of the excitation light ($I_{\rm pump}$) for two limiting cases (steady-state and instantaneous limit), taking into account the generation, relaxation, diffusion, and radiative and non-radiative decays of 1-D excitons in SWNTs. The fitting of the developed model to the experimentally obtained $I_{\rm PL}$ vs. $I_{\rm pump}$ curves allowed us to quantitatively estimate the exciton density for a given average diffusion length within the spontaneous decay lifetime $l_{\rm x}$ (or, for a given diffusion constant D if the spontaneous decay lifetime is known). The solution for the instantaneous limit [Eq. (15)] was compared with a Monte Carlo simulation, from which the validity of the developed model was confirmed. It was shown that the solution obtained based on the conventional mean-field rate equation [Eq. (17)] qualitatively disagrees with the experimental results in the high saturation regime, which is considered to be due to the inherent collapse of this assumption for 1-D excitons. The approaches introduced in this paper are suggested to be used for correctly describing the saturation behaviors of the PL from excitons in SWNTs.

Acknowledgments

The author thanks Junichiro Kono and Ajit Srivastava for discussions, and acknowledges Erik Einarsson for an emendation. Part of this work was financially supported by Grants-in-Aid for Scientific Research (#18-09883) from the Japan Society for the Promotion of Science (JSPS).

[1] T. Ogawa and Y. Kanemitsu, eds., *Optical Properties of Low-Dimensional Materials* (World Scientific Publishing Co., Singapole, 1995).
[2] T. Giamarchi, *Quantum Physics in One Dimension* (Oxford University Press, New York, 2004).
[3] R. S. Knox, *Theory of Excitons* (Achademic Press, New York, 1963).
[4] T. Ogawa and T. Takagahara, Phys. Rev. B **43**, 14325 (1991); *ibid.* **44**, 8138 (1991).
[5] F. Rossi and E. Molinari, Phys. Rev. Lett. **76**, 3642 (1996).
[6] E. Kapon, D. M. Hwang, and R. Bhat, Phys. Rev. Lett. **63**, 430 (1989).
[7] W. Wegscheider, L. N. Pfeiffer, M. M. Dignam, A. Pinczuk, K. W. West, S. L. McCall, and R. Hull, Phys. Rev. Lett. **71**, 4071 (1993).
[8] R. Ambigapathy, I. Bar-Joseph, D. Y. Oberli, S. Haacke, M. J. Brasil, F. Reinhardt, E. Kapon, and B. Deveaud, Phys. Rev. Lett. **78**, 3579 (1997).
[9] S. D. Sarma and D. W. Wang, Phys. Rev. Lett. **84**, 2010 (2000).
[10] D. W. Wang and S. D. Sarma, Phys. Rev. B **64**, 195313 (2001).
[11] J. Rubio, L. Pfeiffer, M. H. Szymanska, A. Pinczuk, S. He, H. U. Baranger, P. B. Littlewood, K. W. West, and B. S. Dennis, Solid State Commun. **120**, 423 (2001).
[12] H. Akiyama, L. N. Pfeiffer, M. Yoshita, A. Pinczuk, P. B. Littlewood, K. W. West, M. J. Matthews, and J. Wynn, Phys. Rev. B **67**, 041302 (2003).
[13] T. Guillet, R. Grousson, V. Voliotis, M. Menant, X. L. Wang, and M. Ogura, Phys. Rev. B **67**, 235324 (2003).
[14] Y. Hayamizu, M. Yoshita, Y. Takahashi, H. Akiyama, C. Z. Ning, L. N. Pfeiffer, and K. W. West, Phys. Rev. Lett. **99**, 167403 (2007).
[15] Q.-H. Xu, D. Moses, and K. W. West, Phys. Rev. B **68**, 174303 (2003).
[16] G. Dicker, M. P. de Haas, and L. D. A. Siebbeles, Phys. Rev. B **71**, 155204 (2005).
[17] Y. Zaushitsyn, K. G. Jespersen, L. Valkunas, V. Sundstrom, and A. Yartsev, Phys. Rev. B **75**, 195201 (2007).
[18] S. M. King, D. Dai, C. Rothe, and A. P. Monkman, Phys. Rev. B **76**, 085204 (2007).
[19] F. Wang, G. Dukovic, E. Knoesel, L. E. Brus, and T. F. Heinz, Phys. Rev. B **70**, 241403 (2004).
[20] G. N. Ostojic, S. Zaric, J. Kono, V. C. Moore, R. H. Hauge, and R. E. Smalley, Phys. Rev. Lett. **94**, 097401 (2005).
[21] Y.-Z. Ma, L. Valkunas, S. L. Dexheimer, S. M. Bachilo, and G. R. Fleming, Phys. Rev. Lett. **94**, 157402 (2005).
[22] S. Iijima and T. Ichihashi, Nature **363**, 603 (1993).
[23] A. Jorio and G. Dresselhaus and M. Dresselhaus, eds., *Carbon Nanotubes: Advanced Topics in the Synthesis, Structure, Properties and Applications* (Springer, Berlin, 2008).
[24] C. D. Spataru, S. Ismail-Beigi, L. X. Benedict, and S. G. Louie, Phys. Rev. Lett. **92**, 077402 (2004).
[25] V. Perebeinos, J. Tersoff, and P. Avouris, Phys. Rev. Lett.

92, 257402 (2004).
[26] F. Wang, G. Dukovic, L. E. Brus, and T. F. Heinz, Science **308**, 838 (2005).
[27] J. Maultzsch, R. Pomraenke, S. Reich, E. Chang, D. Prezzi, A. Ruini, E. Molinari, M. S. Strano, C. Thomsen, and C. Lienau, Phys. Rev. B **72**, 241402 (2005).
[28] D. Moses, J. Wang, A. J. Heeger, N. Kirova, and S. Brazovski, Proc. Natl. Acad. Sci. **98**, 13496 (2001).
[29] Y. Murakami and J. Kono (2008), ArXiv:0804.3190v1.
[30] C.-X. Sheng, Z. V. Vardeny, A. B. Dalton, and R. H. Baughman, Phys. Rev. B **71**, 125427 (2005).
[31] R. M. Russo, E. J. Mele, C. L. Kane, I. V. Rubtsov, M. J. Therien, and D. E. Luzzi, Phys. Rev. B **74**, 041405 (2006).
[32] L. Cognet, D. A. Tsyboulski, J. R. Rocha, C. D. Donyle, J. M. Tour, and R. B. Weisman, Science **316**, 1465 (2007).
[33] A. Suna, Phys. Rev. B **1**, 1716 (1970).
[34] D. C. Torney and H. M. McConnell, J. Phys. Chem. **87**, 1941 (1983).
[35] D. Toussaint and F. Wilczek, J. Chem. Phys. **78**, 2642 (1983).
[36] V. Privmann, C. R. Doering, and H. L. Frisch, Phys. Rev. E **48**, 846 (1993).
[37] J. Cardy and U. C. Tauber, Phys. Rev. Lett. **77**, 4780 (1996).
[38] D. ben-Avraham, Phys. Rev. Lett. **81**, 4756 (1998).
[39] T. O. Masser and D. ben-Avraham, Phys. Rev. E **64**, 062101 (2001).
[40] Y. Miyauchi and S. Mauyama, Phys. Rev. B **74**, 035415 (2006).
[41] C. Manzoni, A. Gambetta, E. Menna, M. Meneghetti, G. Lanzani, and G. Cerullo, Phys. Rev. Lett. **94**, 207401 (2005).
[42] T. Hertel, V. Perebeinos, J. Crochet, K. Arnold, M. Kappes, and P. Avouris, Nano Lett. **8**, 87 (2008).
[43] S. Lebedkin, F. Hennrich, O. Kiowski, and M. M. Kappes, Phys. Rev. B **77**, 165429 (2008).
[44] G. N. Ostojic, S. Zaric, J. Kono, M. S. Strano, V. C. Moore, R. H. Hauge, and R. E. Smalley, Phys. Rev. Lett. **92**, 117402 (2004).
[45] F. Wang, G. Dukovic, L. E. Brus, and T. F. Heinz, Phys. Rev. Lett. **92**, 177401 (2004).
[46] S. Reich, M. Dworzak, A. Hoffmann, C. Thomsen, and M. S. Strano, Phys. Rev. B **71**, 033402 (2005).
[47] The choice of these D and $\tau_{\rm tot}$ values was based on the suggestion made by Ref. 32, based on which "$l_{\rm x} = 45$ nm" in this report has also been chosen. Hence, the comparison of the model and the simulation here was done in an inconsistent manner.
[48] L. Valkunas, G. Trinkunas, V. Liuolia, and G. Grondelle, Biophys. J. **69**, 1117 (1995).
[49] T. W. Roberti, N. J. Cherepy, and J. Z. Zhang, J. Chem. Phys. **108**, 2143 (1998).
[50] K. E. O'Hara, L. O. Suilleabhain, and J. P. Wolfe, Phys. Rev. B **60**, 10565 (1999).